JOURNAL SECTION: Cognitive Neuroscience

Spatially resolved time-frequency analysis of odour coding in the insect antennal lobe

Marco Paoli[1], Nathan Weisz[1,2], Renzo Antolini[1,3], Albrecht Haase[1,3]

[1] Center for Mind/Brain Sciences, University of Trento, Trento, Italy

[2] Centre for Cognitive Neuroscience and Division of Physiological Psychology, University of Salzburg, Austria

[3] Department of Physics, University of Trento, Trento, Italy

Correspondence:

Marco Paoli, Center for Mind/Brain Sciences, University of Trento, Piazza Manifattura 1, 38068 Rovereto (TN), Italy. Email: marco.paoli@unitn.it;

Albrecht Haase, Center for Mind/Brain Sciences, University of Trento, Piazza Manifattura 1, 38068 Rovereto (TN), Italy. Email: albrecht.haase@unitn.it.

Running title: Odorant-induced oscillatory modulation

Number of pages: 23; Number of figures: 7; Number of Words: 195 (Abstract), 508 (Introduction), 5496 (whole manuscript)

Keywords: time-frequency analysis, sensory coding, two-photon microscopy, honeybee

Abstract

Antennal lobes constitute the first neurophils in the insect brain involved in coding and processing of olfactory information. With their stereotyped functional and anatomical organization, they provide an accessible model with which to investigate information processing of an external stimulus in a neural network *in vivo*. Here, by combining functional calcium imaging with time-frequency analysis, we have been able to monitor the oscillatory components of neural activity upon olfactory stimulation. The aim of the present study is to investigate the presence of stimulus-induced oscillatory patterns in the honeybee antennal lobe, and to analyse the distribution of those patterns across the antennal lobe glomeruli. Fast two-photon calcium imaging reveals the presence of low-frequency oscillations, the intensity of which is perturbed by an incoming stimulus. Moreover, analysis of the spatial arrangement of this activity indicates that it is not homogeneous throughout the antennal lobe. On the contrary, each glomerulus displays an odorant-specific time-frequency profile, and acts as a functional unit of the oscillatory activity. The presented approach allows simultaneous recording of complex activity patterns across several nodes of the antennal lobe, providing the means to better understand the network dynamics regulating olfactory coding and leading to perception.

Introduction

Insect brains provide an accessible model to investigate chemosensory reception and representation. In particular, studies of their olfactory circuits have been of paramount importance in understanding the spatio-temporal nature of odour coding (Wehr & Laurent, 1996; Joerges *et al.*, 1997). The honeybee olfactory circuit architecture comprises three functional and anatomical layers: the antennae, which are the sensory organs; the antennal lobes (ALs), the primary processing centres and functional equivalent of the vertebrate

olfactory bulb; and the mushroom bodies (MBs) and lateral protocerebrum, higher-order sensory integration centres (Galizia, 2014). Briefly, odorants are received at the periphery by the olfactory receptor neurons (ORNs), each expressing a single olfactory receptor (OR) and transmitting the elicited signal to the antennal lobe. Each AL receives the raw olfactory signal, processes it through a network of ≈4000 local interneurons, and relays the resulting information to ≈800 projection neurons (PNs). The antennal lobes are composed by 165 glomeruli, which are functional and anatomical units, each receiving direct input from a single ORN type. Finally, PNs convey the signal from the AL glomeruli to the MB and lateral protocerebrum, where the information is sparsely distributed across thousands of synapses, and then integrated with other sensory inputs and pre-existing information (Galizia, 2014).

During the past 20 years, odour representation in the AL has been widely investigated by using wide-field fluorescent microscopy to probe calcium activity via bulk or intracellular staining with calcium-sensitive dyes (Galizia & Menzel, 2000; Hourcade *et al.*, 2009; Girardin *et al.*, 2013). Whereas intracellular recordings already indicated a distributed odour representation and a neuron-odorant specificity (Sun *et al.*, 1993; Wehr & Laurent, 1996), functional calcium imaging allowed simultaneous observation of the odour elicited activity across a whole AL cross-section. This led to a further understanding of the combinatorial nature of peripheral odour coding in the honeybee, allowing the identification of distinct odour response patterns, which are maintained across multiple stimulations and across individuals (Joerges *et al.*, 1997; Galizia *et al.*, 1999). The introduction of fast laser scanning two-photon microscopy for functional calcium imaging dramatically increased the signal sampling rate from 10 Hz to up to 500 Hz (Haase *et al.*, 2010; Paoli *et al.*, 2016), providing the means to apply optical tools to investigate also the dynamics of odour coding.

Here, analogous to EEG/MEG studies, we have investigated the effects of an external sensory input on a neural network *in vivo*, decoding calcium-imaging signals using a time-

frequency (TF) analysis approach. Intracellular calcium concentration is a known indicator of neural activity and, although the duration of calcium signals and action potentials are different, the two signals are highly correlated (Galizia & Kimmerle, 2004; Moreaux & Laurent, 2007). This makes it possible to study the oscillatory activity of a neural network by analysing calcium signal dynamics (Galán *et al.*, 2006; Moreaux & Laurent, 2007; Grewe *et al.*, 2010).

In the present study, we exposed honeybees to multiple-trial odour stimuli and recorded calcium-dependent fluorescence variation in the AL. Acquired signals were analysed in both the time and frequency domains, and stimulus-induced frequency power modulations have been characterized.

Materials and methods

Staining and preparation procedure

Forager honeybees (*Apis mellifera*) were collected between February and June from outdoor beehives. Animal preparation for calcium imaging consists of a two-day procedure (Galizia *et al.*, 1999). On the first day, bees are placed in a custom-made Plexiglas mount, and the head is stabilized with soft dental wax. A small window in the head cuticle is opened. Glands and tracheae covering the site of injection are displaced. The tip of a borosilicate glass needle covered with Fura-2-dextran (ThermoFisher Scientific) is inserted between the mushroom body calices, below the alpha lobe, and kept in place until the dye crystal dissolves (Fig. 1). After the staining procedure, the head capsule is closed and sealed. Bees are then fed *ad libitum* with 50% sucrose/water solution and kept in a dark, moist place while the dye diffuses retrograde into the AL. On the second day, the cuticle is re-opened, glands

and tracheae are removed, and the antennal lobes are exposed. Haemolymph in excess is removed, and the brain is covered in a transparent two-component silicon (Kwik-Sil, WPI).

Olfactory stimulation

Olfactory stimulation was performed with a custom-built, computer-controlled olfactometer inspired by an instrument used by Szyzska and colleagues (Szyszka *et al.*, 2011). The mechanical apparatus comprises 8 symmetrical channels, each loaded with two Teflon-sealed glass vials: one containing 1 mL of mineral oil-diluted odorant; one containing 1 mL of pure mineral oil. All channels receive the same airflow and converge into a nosepiece facing the honeybee. Valves switch between odour and blank channels. Continuous air suction behind the bee clears residual odours. The array of valves is operated via tailored electronics by a PCIe-6321 multifunction board (National Instruments). LabVIEW-based custom-made software synchronizes stimulus delivery and microscopy acquisition with a precision of <10 ms. In this study, the following odorants were employed for the olfactory stimulation experiments: 1-octanol, benzaldehyde, acetophenone, isoamyl acetate, and 1-hexanol (Sigma-Aldrich). Each odour was freshly prepared weekly and presented in a 1:500 dilution in mineral oil. During stimulation the bee was exposed for 30 trials to the same stimulus in a 5/25 s ON/OFF configuration. **Of 12 analysed honeybees, 2 were exposed to four different odorants, 3 to two odorants, 7 to one odorant. In a second instance, a single honeybee was exposed to 5 different odorants for a direct comparison of odour response specificity across many odorants. The data acquired from this single experiment are discussed in detail in Figure 5 and in Supplementary Figures 1 and 2**.

Two-photon optical imaging

The optical setup consists of a two-photon microscope (Ultima IV, Bruker) combined with an ultra-short pulsed laser (Mai Tai Deep See HP, Spectra-Physics-Newport) tuned to 800 nm for Fura-2 excitation. Freely programmable galvanometric mirrors allow for fast and variable scanning. All images were acquired using a 20× water-immersion objective (NA 1.0, Olympus). The fluorescence was collected in epi-configuration, separated by a dichroic mirror (Chroma Technology Corporation), filtered by a 70 nm band-pass centred at 525 nm, and detected by photomultiplier tubes (Hamamatsu Photonics). Optimal signal-to-noise ratio was achieved with laser power of ≈10 mW without any indication of photo-bleaching, even after repeated exposure. Functional data acquisition was performed scanning along a custom 1D trajectory at 50 Hz. To avoid any bias due to anatomical and functional asymmetries (Rigosi *et al.*, 2011, 2015), all imaging experiments were conducted on the right AL.

Signal processing and statistical analysis

Data analysis was performed automatically with custom-made algorithms based on FieldTrip, a Matlab software toolbox developed for EEG and MEG data analysis (Oostenveld *et al.*, 2011). The time interval from 4.5 to 0.5 s pre-stimulus has been used for baseline subtraction. Calcium-response data have been normalized by the fluorescence background (-Δ*F*/*F*), and averaged across all trials, unless stated otherwise. Average response activity is calculated in the [0 , 0.8] s window after stimulus onset. Moreover, each independent trial has been analysed in the time-frequency domain by convolution with complex Morlet wavelets of the form

$$w(t,f) = \left(\sigma_t\sqrt{x}\right)^{-\frac{1}{2}} \exp\left(\frac{-t^2}{2\sigma_t^2}\right) \exp(i2\pi f t)$$

These wavelets have Gaussian envelops in time and frequency, but, in contrast to a classical moving Fourier transform, their frequency bandwidth $\sigma_f = 1/(2\pi\sigma_t)$ is not constant, but increases linearly with the central frequency f. Thus, all wavelets contain a fixed number of cycles, in our case $2f/\sigma_f = 7$. We analysed a frequency range from 1 to 20 Hz. The upper frequency limit is dictated by the physiological Ca^{2+} dynamics, where signals rise quickly (<5 ms), but decay in 50 - 100 ms (Helmchen *et al.*, 1996). Resulting power spectra have been averaged across trials and presented in dB scale (*i.e.* logarithmic spectral difference from baseline). When an averaged low-frequency power is considered, the mean is computed between 1.5 and 5 Hz. The stimulus-induced power attenuation is studied between 0.8 and 5 s after stimulus onset.

Odorant specificity of glomerular response maps was shown qualitatively for 3 honeybees and quantified exemplarily for a honeybee stimulated with 5 different odorants. Via exploratory data analysis a subset of N=9 glomeruli was found to be activated by at least one of the tested odorants, thus contributing to the analysed odour code. Odour specificity of glomerular responses was then assayed by two-way ANOVA with factors Glomerulus and Odour, analysing N=10 experimental trials. Simple effects between single odour codes were compared pairwise with two-tailed Student's t-tests ($\alpha = 0.05$; Bonferroni corrected).

Results

The following results are based on the olfactory stimulation and functional imaging analysis of 12 honeybees. Each honeybee was exposed 30 times to the same odorant and, when possible, more than one odour was tested on the same animal. This led to a total of 21 subject/odour combinations. The multiple-stimulus protocol is a standard procedure adopted in functional imaging experiments to discriminate odour-induced calcium variations from spontaneous activity. Thus, the amplitude of the calcium signal averaged over multiple

trials represents a measure of the neuronal response to an odorant cue in a selected glomerulus. This operation strongly enhances those responses, which are phase-locked with stimulus onset, but drastically attenuates the relative contribution of signal oscillations that are not phase-locked with the odour pulse (Fig. 2). This effect is well known from the analysis of human electrophysiological data, *e.g.* EEG and MEG (Tallon-Baudry & Bertrand, 1999). To access also these oscillatory components of the AL network activity, we performed a continuous wavelet transformation of the calcium-imaging data, analysing the stimulus-related activity in the time-frequency domain.

Time-frequency analysis of calcium signals in the AL projection neurons revealed a strong odour-induced intensity modulation at low frequencies, from 1.5 to 5 Hz, consistently across individuals and for all tested odorants. In particular, a broadband power increase was observed at stimulus onset (t=0), which is the frequency decomposition of the sharp fluorescence change in responsive glomeruli. A more interesting effect was detected after odour onset: a marked power decrease in the considered frequency range. This effect was observed in all tested animals, with variation in intensity and in duration. In some cases, the effect lasted for the whole stimulation window; in other cases, it outlasted the stimulus offset by more than 2 seconds (Fig. 2 and 3).

Next, we assessed the spatial distribution of the observed stimulus-induced power decrease. In particular, we investigated whether this effect is homogeneous throughout the whole AL. Fast-scanning two-photon microscopy allows optical recording of thousands of pixels with a high sampling rate. By continuous wavelet transform, we computed the power spectrum of any region of interest within the field of view, *i.e.* a complete AL cross-section. Hence, we compared the time-frequency spectra across different AL glomeruli (Fig. 4). Notably, such comparison was performed on signals generated in different regions of the AL, but during the same imaging experiment, thus simultaneously acquired. This analysis

clearly showed that the low-frequency modulation induced by an olfactory stimulation is highly heterogeneous across AL projection neurons. In fact, some of the glomeruli showed no change in their oscillatory pattern, while others showed clear odour-induced responses in the TF domain (Fig. 4 and 5). Considering that glomeruli are anatomical and functional units of the AL, our prediction was that the diverse response patterns would be homogeneous within the same glomerulus. Indeed, power spectra generated from different regions of the same glomerulus are clearly comparable and display the same frequency modulations. By contrast, regions of the AL close in space but belonging to different glomeruli can show different power spectra (Fig. 4).

Different odorants are represented within the antennal lobe with different patterns of glomerular activation. Considering that the low-frequency activity modulation is spatially heterogeneous and glomerulus-specific, we investigated whether the elicited time-frequency profile, as well as the calcium signal amplitude, is odorant-specific. **For this purpose, a honeybee was sequentially exposed to all 5 tested odorants (*N*=10 repetitions), and odour response maps were calculated both in time and time-frequency domains. Mean odour response profiles across 9 glomeruli are shown (Supplementary Figures 1 and 2)**. Statistical significance of two factors, glomerulus and odorant, on the induced responses was assayed with a two-way ANOVA, revealing significant main effects of both factors and a significant interaction (Factor Glomerulus: $F_{8,405} = 3.67$, $p = 4*10^{-4}$; Factor Odorant: $F_{4,405} = 3.45$, $p = 9*10^{-3}$; Interaction Glomerulus/Odorant: $F_{32,405} = 6.13$, $p < 10^{-19}$). Effects between odour pairs were analysed by multiple *t*-tests (Fig. 5). This analysis clearly shows that the stimulus-related frequency modulation is odorant dependent. Furthermore, as confirmed by the significant interaction, two odorants can trigger similar responses in certain glomeruli and different responses in others, supporting the concept of odorant-specific response maps also in the time-frequency domain. **Also, comparisons of the**

stimulus-elicited glomerular responses in the time and in the time-frequency domains across odorants are displayed in Supplementary Figures 3-5. Here, the odour specific responses of three different honeybees to two distinct odorants are shown. This analysis further confirms the odour specificity of the low-frequency power attenuation.

Finally, we considered all functional units from the 12 analysed bees (*N*=497) and investigated the relationship between the stimulus-evoked calcium signal (mean fluorescence intensity during the first 800 ms after stimulus onset), and the frequency modulation in the [1.5 , 5] Hz range during two temporal windows with respect to stimulus onset: early [-0.8 , 0.8] s and late [0.8 , 5] s. This analysis indicated a positive correlation (R^2=0.59, *N*=497) between the fluorescence signal intensity and the low-frequency power increase observed at stimulus onset. By contrast, no correlation was detected between the evoked calcium activity and the induced low frequency power variation observed during olfactory stimulation (R^2=0.12, *N*=497) (Fig. 6).

Discussion

Odour representation in the insect antennal lobe has been extensively described in terms of specific activation or inhibition of its functional units (Joerges *et al.*, 1997; Galizia *et al.*, 1999; Wang *et al.*, 2003; Zube *et al.*, 2008). However, in these studies on olfactory coding, sampling rates were limited to 4 - 6 Hz, precluding analysis of the fine dynamics of odour-elicited responses (Galizia *et al.*, 2000; Sachse & Galizia, 2002). Hence, functional imaging analysis of olfactory coding in insects has been focused on intensity and spatial distribution of stimulus-evoked events, which are phase-locked to the stimulus onset and observable at a low sampling rate. However, such analyses ignore any information on stimulus-induced oscillatory activities that are not in phase with stimulus onset (Tallon-

Baudry & Bertrand, 1999). Analyses of oscillatory patterns of brain activity in insects have been generally conducted via single-cell or local field potential recordings (Matsumoto & Hildebrand, 1981; Christensen *et al.*, 2003; Stopfer *et al.*, 2003; Cassenaer & Laurent, 2007). These methods allow precise characterization of the stimulus-related activity in individual neurons or in selected anatomical compartments, but have limited capability to monitor multiple regions at high spatial resolution. This can be partially overcome by the use of multiple-electrode arrays (Lam *et al.*, 2000). **However, this technique offers relatively low spatial resolution, and it is not optimal for simultaneous frequency analysis at the level of a neural network.** Here, by combining fast-scanning functional calcium imaging with time-frequency analysis, we implemented an optical approach that overcomes these limitations, and allows for simultaneous investigation of oscillatory activity across multiple regions of the antennal lobe at 1-µm-resolution.

Odour-induced modulation of low-frequency oscillations

In mammalian and insect brains, networks of neurons generate oscillatory waves of activity associated with both signal processing and neural connectivity (Laurent, 2002; Buzsáki *et al.*, 2012, 2013; Kay, 2015). In the present study, we have identified a frequency band between 1.5 and 5 Hz, whose intensity in the antennal lobe decreases upon olfactory stimulation. In particular, we detected a power attenuation commencing at stimulus onset and lasting the entire stimulation period. The effect is not time-locked to the stimulus onset and cannot be observed upon multiple-trial averaging of the activity time curves. In frequency space instead, temporal jitter is transformed into phase factors and the analysis of power spectra eliminates these phase factors. Hence, the induced activity is conserved also after averaging the power spectra. Notably, this effect was found in all studied individuals and for all tested odorants. In particular, we report that when stimulating an individual honeybee with multiple odorants, each stimulus triggers a different time-frequency

response pattern across the analysed glomeruli. This finding clearly indicates that the detected phenomenon is not a generic response to an incoming olfactory input, but it is a specific response of the **antennal lobe PNs** to a particular odorant. Oscillatory activity in this frequency range has already been identified in the fruit fly brain by local field potential recordings (Paulk *et al.*, 2013). However, Paulk and colleagues regarded those frequencies as non-informative, because they were probably generated by the insect heart rate of about 3 Hz (Robbins *et al.*, 1999). Here, we have been able to show that this frequency modulation is strictly related to olfactory stimulation and is heterogeneously distributed across the AL. Modulation of spontaneous activity of the antennal lobe projection neurons in presence of olfactory stimulation has already been reported by Galan and colleagues (Galán *et al.*, 2006). Investigating spontaneous activity patterns before and after odorant exposure, they observed that although the overall neural activity remains constant, the degree of correlation between apparently spontaneous activities was significantly affected following the Hebbian rule, *i.e.* pairs of glomeruli which were both excited or inhibited by the stimulus increased their spontaneous activity coherence. Indeed, a transient synchronization of the spontaneous activity between two glomeruli would affect their oscillatory profile, potentially inducing a partial power loss in certain frequency components. Also, this effect persists after stimulus offset and could explain an oscillatory activity modulation outlasting the stimulation window.

The oscillatory power decay observed upon stimulation indicates that a continuous ≈3 Hz oscillatory activity in the PNs population is transiently interrupted during the process of odour reception. This phenomenon may reflect resting state activity of projection neurons, a signal component generally enhanced in the absence of an explicit stimulation (Rosazza & Minati, 2011; Lange *et al.*, 2014). Notably, the presence of endogenous oscillatory activity in the AL, locally attenuated during stimulus processing, is – at least at a superficial level –

reminiscent of the alpha waves (8-12 Hz; (Buzsáki *et al.*, 2013; Lange *et al.*, 2014)). Moreover, the attenuation of this ≈3 Hz oscillatory activity may be offset by a synchronization of the neurons at different frequencies, outside the working range of the current analysis. In this regard, electrophysiological studies revealed the presence of a 20-40 Hz odour-evoked synchronization of firing in insect antennal lobes and mushroom bodies (Laurent & Naraghi, 1994; MacLeod & Laurent, 1996; Stopfer *et al.*, 1997; Okada & Kanzaki, 2001; Ito *et al.*, 2009; Cassenaer & Laurent, 2012; Paulk *et al.*, 2013). Among the others, Denker and colleagues investigated the modulation of PNs oscillatory activity during olfactory stimulation in honeybee (Denker *et al.*, 2010). Their study reports an increase in the ≈50 Hz oscillatory power at stimulus onset followed by an adjustment of the main oscillatory component at slightly lower frequencies. Although the reported activity lays outside of our working range, it indicates the presence of a stimulus induced modulation of the resting state activity associated with olfactory coding and associative plasticity in the honeybee AL. It will be interesting to investigate to what extent the described low frequency modulation may be affected by "cognitive" factors, going beyond the information provided by the evoked parts of the signals, a pattern that has been frequently described in humans (Siegel *et al.*, 2012).

Oscillatory activity is spatially structured

By means of spatially resolved TF analysis, we have investigated the consistency of low-frequency oscillatory activity across the AL. We have studied the variability of its oscillatory power intensity within each glomerulus and across glomerular borders, revealing that each glomerulus has a specific TF response profile. As a result, we identified the glomeruli as the functional units of this oscillatory activity. **The heterogeneity of the spatiotemporal activity patterns across the honeybee AL projection neuron population has already been suggested by Stopfer and colleagues** (Stopfer *et al.*, 1997, 2003)**. By means of single-PN recordings, they revealed that not all measured cells**

show the same activity pattern in response to a certain olfactory cue(Stopfer *et al.*, 2003)**.** In addition, Okada and Kanzaki used a voltage-sensitive dye and performed optical recordings of odour-induced activity in the bumblebee AL (Okada & Kanzaki, 2001). Their study is one of the few that combines optical imaging with the analysis of signals in the TF domain, allowing the visualization of the elicited activity simultaneously across a large portion of the AL. They observed that oscillatory signals are not homogeneously distributed across the AL, but organized in domains of the size of one or of a few glomeruli. We were now able to resolve this heterogeneity to follow the glomerular structure.

Moreover, we report that the oscillatory pattern modulation does not reflect an excitatory or inhibitory glomerular response. A low-frequency power depression can be observed upon glomerular inhibition, excitation, or even in absence of detectable sustained change in intracellular calcium concentration (Fig. 2 and 4, Supplementary Figures 3-5). Hence, glomeruli that appear as non-responsive when analysed in the temporal domain may reveal an odour-elicited response in the time-frequency domain. Furthermore, as schematically depicted in Fig. 7, the power distribution of such oscillatory activity across the AL is different from the odour-response pattern conventionally measured as the amplitude of the fluorescence change upon stimulation. Within this frame, studying the odour-elicited glomerular activity in the time-frequency domain will provide access to previously neglected information on olfactory coding and signal processing.

Concluding remarks

In this study, high spatial and temporal resolution calcium imaging data have been subjected to time-frequency analysis allowing the observation of the signal frequency components across multiple glomeruli at once. This approach revealed the presence of a spatially structured oscillatory activity in the honeybee antennal lobe.

Such low-frequency activity pattern is modulated by an olfactory stimulation and displays a spatially heterogeneous distribution, which is both odorant- and glomerulus-specific. Notably, this is the first characterization of such a phenomenon. Future challenges will be investigating the origin and the functional role of these oscillations. This will give us better understanding into the neural mechanisms behind the perception of an incoming stimulus in a sensory circuit. At the same time, correlation analyses of the oscillatory patterns across multiple AL glomeruli will provide better insight into the static and dynamic properties of the network's architecture.

Acknowledgements

This work was supported by the University of Trento (Strategic project P.STR.14 BEES). The authors declare no conflict of interests. We gratefully thank B. Timberlake for proofreading the manuscript.

Abbreviations

AL, antennal lobe; EEG, electroencephalography; MEG, magnetoencephalography; MB, mushroom body; OR, odorant receptor; ORN, odorant receptor neuron; PN, projection neuron; TF, time-frequency.

References

Buzsáki, G., Anastassiou, C.A., & Koch, C. (2012) The origin of extracellular fields and currents--EEG, ECoG, LFP and spikes. *Nat. Rev. Neurosci.*, **13**, 407–420.

Buzsáki, G., Logothetis, N., & Singer, W. (2013) Scaling brain size, keeping timing: evolutionary preservation of brain rhythms. *Neuron*, **80**, 751–764.

Cassenaer, S. & Laurent, G. (2007) Hebbian STDP in mushroom bodies facilitates the synchronous flow of olfactory information in locusts. *Nature*, **448**, 709–713.

Cassenaer, S. & Laurent, G. (2012) Conditional modulation of spike-timing-dependent plasticity for olfactory learning. *Nature*, **482**, 47–52.

Christensen, T.A., Lei, H., & Hildebrand, J.G. (2003) Coordination of central odor representations through transient, non-oscillatory synchronization of glomerular output neurons. *Proc. Natl. Acad. Sci. U. S. A.*, **100**, 11076–11081.

Denker, M., Finke, R., Schaupp, F., Grün, S., & Menzel, R. (2010) Neural correlates of odor learning in the honeybee antennal lobe. *Eur. J. Neurosci.*, **31**, 119–133.

Galán, R.F., Weidert, M., Menzel, R., Herz, A.V.M., & Galizia, C.G. (2006) Sensory memory for odors is encoded in spontaneous correlated activity between olfactory glomeruli. *Neural Comput.*, **18**, 10–25.

Galizia, C.G. (2014) Olfactory coding in the insect brain: data and conjectures. *Eur. J. Neurosci.*, **39**, 1784–1795.

Galizia, C.G. & Kimmerle, B. (2004) Physiological and morphological characterization of honeybee olfactory neurons combining electrophysiology, calcium imaging and confocal microscopy. *J. Comp. Physiol. A*, **190**, 21–38.

Galizia, C.G. & Menzel, R. (2000) Odour perception in honeybees: coding information in glomerular patterns. *Curr. Opin. Neurobiol.*, **10**, 504–510.

Galizia, C.G., Sachse, S., Rappert, A., & Menzel, R. (1999) The glomerular code for odor representation is species specific in the honeybee Apis mellifera. *Nat. Neurosci.*, **2**, 473–478.

Galizia, C.G.C., Küttner, A., Joerges, J., & Menzel, R. (2000) Odour representation in honeybee olfactory glomeruli shows slow temporal dynamics: an optical recording study using a voltage-sensitive dye. *J. Insect Physiol.*, **46**, 877–886.

Girardin, C.C., Kreissl, S., & Galizia, C.G. (2013) Inhibitory connections in the honeybee antennal lobe are spatially patchy. *J. Neurophysiol.*, **109**, 332–343.

Grewe, B.F., Langer, D., Kasper, H., Kampa, B.M., & Helmchen, F. (2010) High-speed in vivo calcium imaging reveals neuronal network activity with near-millisecond precision. *Nat. Methods*, **7**, 399–405.

Haase, A., Rigosi, E., Trona, F., Anfora, G., Vallortigara, G., Antolini, R., & Vinegoni, C. (2010) In-vivo two-photon imaging of the honey bee antennal lobe. *Biomed. Opt. Express*, **2**, 131–138.

Helmchen, F., Imoto, K., & Sakmann, B. (1996) Ca2+ buffering and action potential-evoked Ca2+ signaling in dendrites of pyramidal neurons. *Biophys. J.*, **70**, 1069–1081.

Hourcade, B., Perisse, E., Devaud, J.-M., & Sandoz, J.-C. (2009) Long-term memory shapes the primary olfactory center of an insect brain. *Learn. Mem.*, **16**, 607–615.

Ito, I., Bazhenov, M., Ong, R.C., Raman, B., & Stopfer, M. (2009) Frequency transitions in odor-evoked neural oscillations. *Neuron*, **64**, 692–706.

Joerges, J., Küttner, A., Galizia, C.G., & Menzel, R. (1997) Representations of odours and odour mixtures visualized in the honeybee brain. *Nature*, **387**, 285–288.

Kay, L.M. (2015) Olfactory system oscillations across phyla. *Curr. Opin. Neurobiol.*, **31**, 141–147.

Lam, Y.W., Cohen, L.B., Wachowiak, M., & Zochowski, M.R. (2000) Odors elicit three different oscillations in the turtle olfactory bulb. *J. Neurosci.*, **20**, 749–762.

Lange, J., Keil, J., Schnitzler, A., van Dijk, H., & Weisz, N. (2014) The role of alpha oscillations for illusory perception. *Behav. Brain Res.*, **271**, 294–301.

Laurent, G. (2002) Olfactory network dynamics and the coding of multidimensional signals. *Nat. Rev. Neurosci.*, **3**, 884–895.

Laurent, G. & Naraghi, M. (1994) Odorant-induced oscillations in the mushroom bodies of the locust. *J. Neurosci.*, **14**, 2993–3004.

MacLeod, K. & Laurent, G. (1996) Distinct mechanisms for synchronization and temporal patterning of odor-encoding neural assemblies. *Science*, **274**, 976–979.

Matsumoto, S.G. & Hildebrand, J.G. (1981) Olfactory Mechanisms in the Moth Manduca sexta: Response Characteristics and Morphology of Central Neurons in the Antennal Lobes. *Proc. R. Soc. B Biol. Sci.*, **213**, 249–277.

Moreaux, L. & Laurent, G. (2007) Estimating firing rates from calcium signals in locust projection neurons in vivo. *Front. Neural Circuits*, **1**, 2.

Okada, K. & Kanzaki, R. (2001) Localization of odor-induced oscillations in the bumblebee antennal lobe. *Neurosci. Lett.*, **316**, 133–136.

Oostenveld, R., Fries, P., Maris, E., & Schoffelen, J.-M. (2011) FieldTrip: Open source software for advanced analysis of MEG, EEG, and invasive electrophysiological data. *Comput. Intell. Neurosci.*, **2011**, 156869.

Paoli, M., Anesi, A., Antolini, R., Guella, G., Vallortigara, G., & Haase, A. (2016) Differential

Odour Coding of Isotopomers in the Honeybee Brain. *Sci. Rep.*, **6**, 21893.

Paulk, A.C., Zhou, Y., Stratton, P., Liu, L., & van Swinderen, B. (2013) Multichannel brain recordings in behaving Drosophila reveal oscillatory activity and local coherence in response to sensory stimulation and circuit activation. *J. Neurophysiol.*, **110**, 1703–1721.

Rigosi, E., Frasnelli, E., Vinegoni, C., Antolini, R., Anfora, G., Vallortigara, G., & Haase, A. (2011) Searching for anatomical correlates of olfactory lateralization in the honeybee antennal lobes: a morphological and behavioural study. *Behav. Brain Res.*, **221**, 290–294.

Rigosi, E., Haase, A., Rath, L., Anfora, G., Vallortigara, G., & Szyszka, P. (2015) Asymmetric neural coding revealed by in vivo calcium imaging in the honey bee brain. *Proc. R. Soc. B Biol. Sci.*, **282**, 20142571.

Robbins, J., Aggarwal, R., Nichols, R., & Gibson, G. (1999) Genetic variation affecting heart rate in Drosophila melanogaster. *Genet. Res.*, **74**, 121–128.

Rosazza, C. & Minati, L. (2011) Resting-state brain networks: Literature review and clinical applications. *Neurol. Sci.*, **32**, 773–785.

Sachse, S. & Galizia, C.G. (2002) Role of inhibition for temporal and spatial odor representation in olfactory output neurons: a calcium imaging study. *J. Neurophysiol.*, **87**, 1106–1117.

Siegel, M., Donner, T.H., & Engel, A.K. (2012) Spectral fingerprints of large-scale neuronal interactions. *Nat. Rev. Neurosci.*, **13**, 121–134.

Stopfer, M., Bhagavan, S., Smith, B.H., & Laurent, G. (1997) Impaired odour discrimination

on desynchronization of odour-encoding neural assemblies. *Nature*, **390**, 70–74.

Stopfer, M., Jayaraman, V., & Laurent, G. (2003) Intensity versus Identity Coding in an Olfactory System. *Neuron*, **39**, 991–1004.

Sun, X.-J., Fonta, C., & Masson, C. (1993) Odour quality processing by bee antennal lobe interneurones. *Chem. Senses*, **18**, 355–377.

Szyszka, P., Demmler, C., Oemisch, M., Sommer, L., Biergans, S., Birnbach, B., Silbering, A.F., & Galizia, C.G. (2011) Mind the gap: olfactory trace conditioning in honeybees. *J. Neurosci.*, **31**, 7229–7239.

Tallon-Baudry, C. & Bertrand, O. (1999) Oscillatory gamma activity in humans and its role in object representation. *Trends Cogn. Sci.*, **3**, 151–162.

Wang, J.W., Wong, A.M., Flores, J., Vosshall, L.B., & Axel, R. (2003) Two-photon calcium imaging reveals an odor-evoked map of activity in the fly brain. *Cell*, **112**, 271–282.

Wehr, M. & Laurent, G. (1996) Odour encoding by temporal sequences of firing in oscillating neural assemblies. *Nature*, **384**, 162–166.

Zube, C., Kleineidam, C.J., Kirschner, S., Neef, J., & Rössler, W. (2008) Organization of the olfactory pathway and odor processing in the antennal lobe of the ant Camponotus floridanus. *J. Comp. Neurol.*, **506**, 425–441.

Figure legends

Figure 1. Calcium sensitive dye injection site. Wide-field microscopy image of an exposed honeybee brain. Fura-2-dextran was injected between the medial (MC) and the lateral calix (LC) of the mushroom bodies (arrowhead). Following the injection, the dye is uptaken by the projection neurons of both antenno-cerebral tracts (l/m-ACT) and retrotransported towards the dendritic ramifications within the glomeruli of the antennal lobe (AL). LH, lateral horn; α, alpha lobe.

Figure 2. Time-frequency analysis. Multiple-trial averaging in the temporal domain (**a**) improves signal-to-noise ratio of stimulus-evoked activity at the expenses of non-phase-locked stimulus-induced events (**b**). Analysis of calcium imaging data ($-\Delta F/F$) in the time-frequency domain (**c**), followed by multiple-trial averaging (**d**), visualizes non-phase-locked stimulus-induced power variations.

Figure 3. Honeybee AL functional calcium imaging. (**a**) Focal plane of honeybee AL was continuously imaged along a 1D freehand linescan at 50 Hz sampling rate; scale bar = 100 µm. (**b**) Profile of stimulus delivery: 5 s OFF / 5 s ON / 5 s OFF. (**c**) Mean fluorescence variation across all channels analysed in the time-frequency domain, and averaged across multiple stimulations. (**d**) Mean oscillatory power in the 1-10 Hz window and (**e**) mean fluorescence intensity profile. Data in (**c-e**) represents the average of N=30 olfactory stimulations.

Figure 4. Fluorescence response to an olfactory stimulation measured in the time and time-frequency domain. Three AL glomeruli have been considered and calcium fluorescence variation and power spectra in three distinct sub-glomerular areas have been compared (**a**). Activity measured in the yellow, green, and blue ROIs are displayed in (**b**),

(**c**), and (**d**) panels respectively. Stimulus was delivered between *t*=0 and *t*=5 s. Scale bar = 100 µm.

Figure 5. Odour specific responses. A honeybee was exposed to 10 repetitions of 5 different odorants. For each stimulus, mean oscillatory power [dB] have been calculated in the [1.5 , 5] Hz / [0.8 , 5] s spectral window. For each glomerulus, odour specificity was analysed by multiple pairwise *t*-tests (α = 0.05; Bonferroni corrected). Results are shown in odour-response correlation matrices. Significant differences in the elicited oscillatory power between two odorants are indicated in black. Used odorants are: 1-octanol, OCT; isoamyl acetate, ISO; 1-hexanol, HEX; acetophenone, ACP; benzaldehyde, BZA.

Figure 6. Analysis of the relationship between fluorescence activity and low frequency intensity variation. (**a**) Example of power spectrum in which the 3 spectral regions of interest are highlighted. Pre-stimulus activity is computed in both time and time-frequency domains in the [-4 , -1] s interval (region R1) (**b**).The calcium-induced fluorescence signal $-\Delta F/F$ is considered in the [0 , 0.8] s window after stimulus onset; the oscillatory power ([1.5 , 5] Hz range) is considered in two different temporal window: [-0.8 , 0.8] s (region R2, **c**) and [0.8 , 5] s (region R3, **d**).

Figure 7. Functional response maps. (**a,b**) Antennal lobe focal plane with and without mask overlay. Identified T1-tract glomeruli are indicated in (**b**). Scale bar = 100 µm. Odour response maps are based on fluorescence change $-\Delta F/F$ (**c**) or on oscillatory power intensity variation (**d**) upon olfactory stimulation. Values are mean of *N*=30 stimulus-elicited responses.

Figure 1:

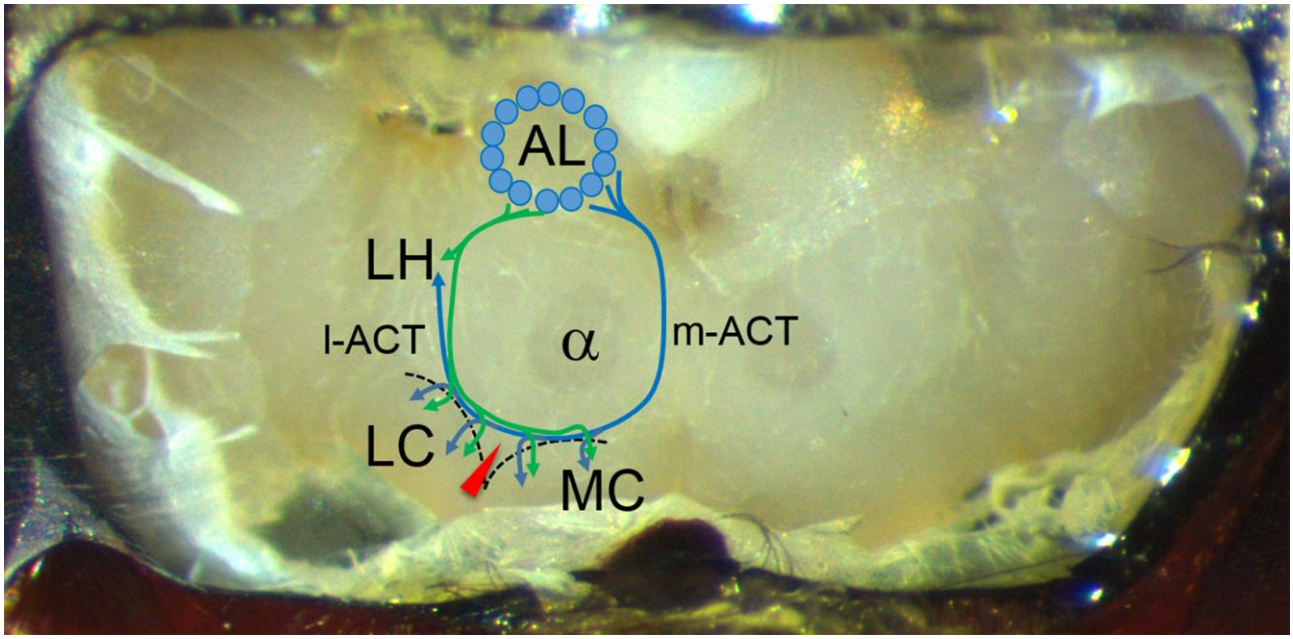

Figure 2:

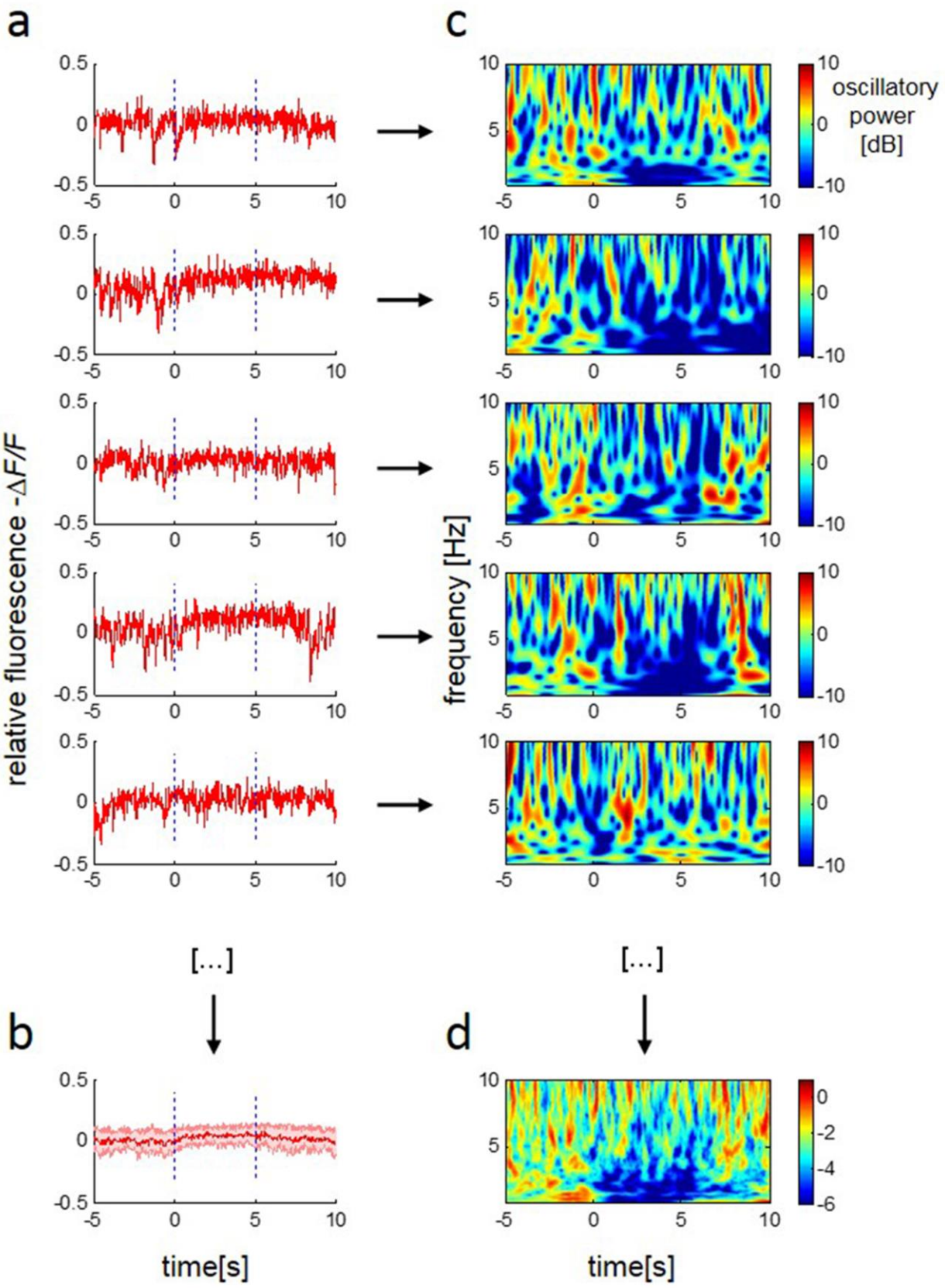
a
c
b
d
relative fluorescence -ΔF/F
frequency [Hz]
oscillatory power [dB]
[…]
[…]
time[s]
time[s]

Figure 3:

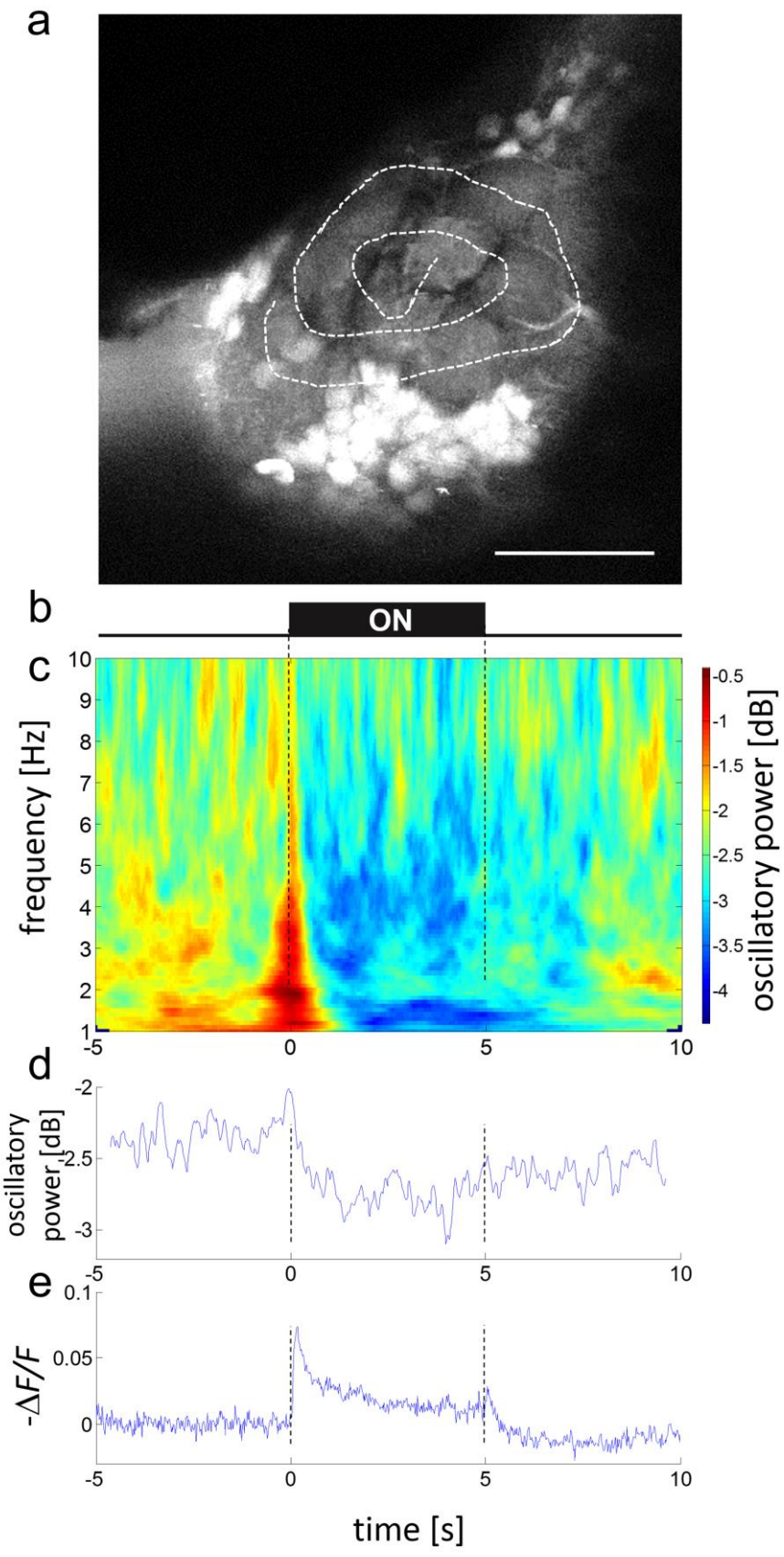
a
b
ON
c
frequency [Hz]
oscillatory power [dB]
d
oscillatory power [dB]
e
-ΔF/F
time [s]

Figure 4:

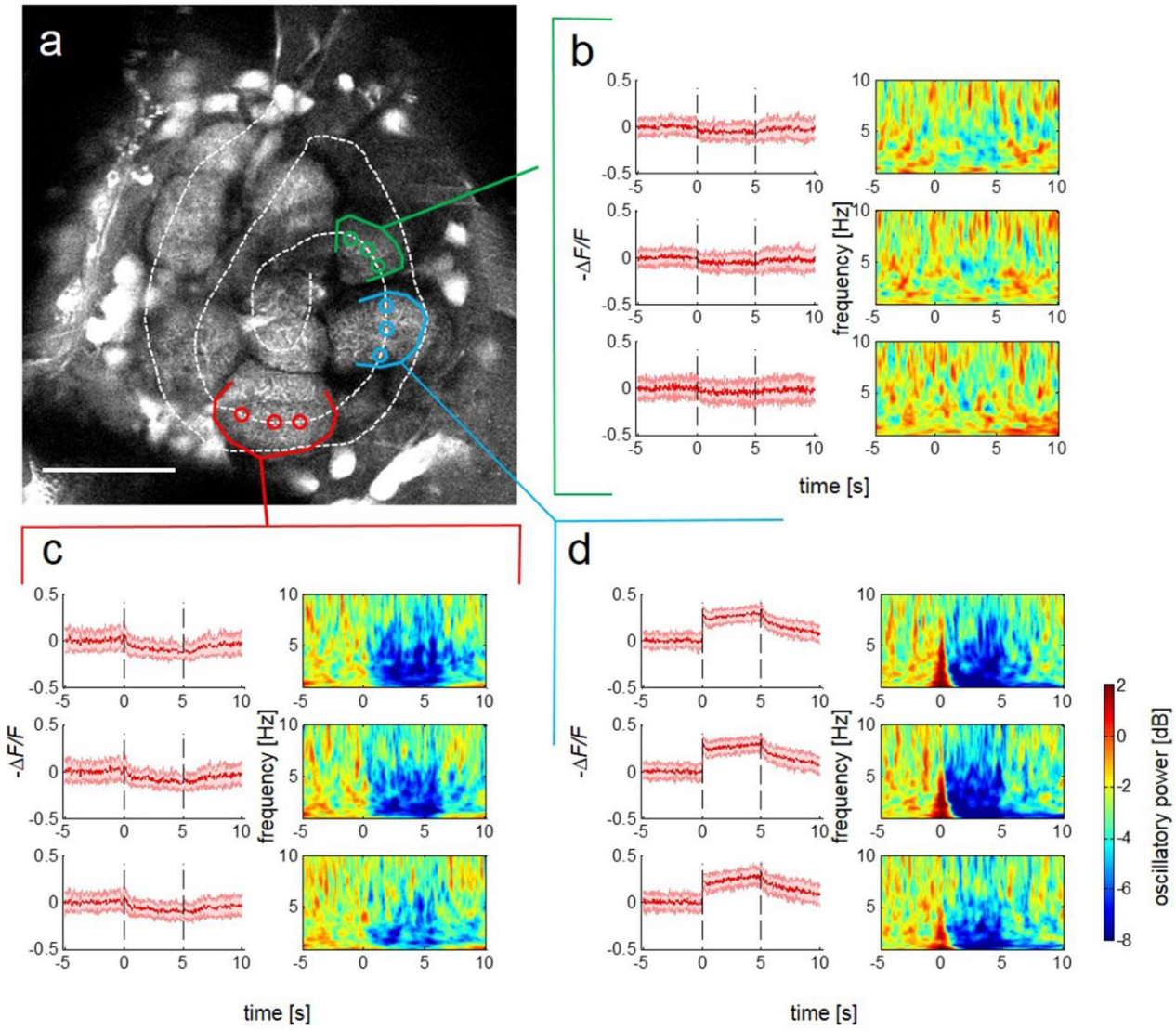

Figure 5:

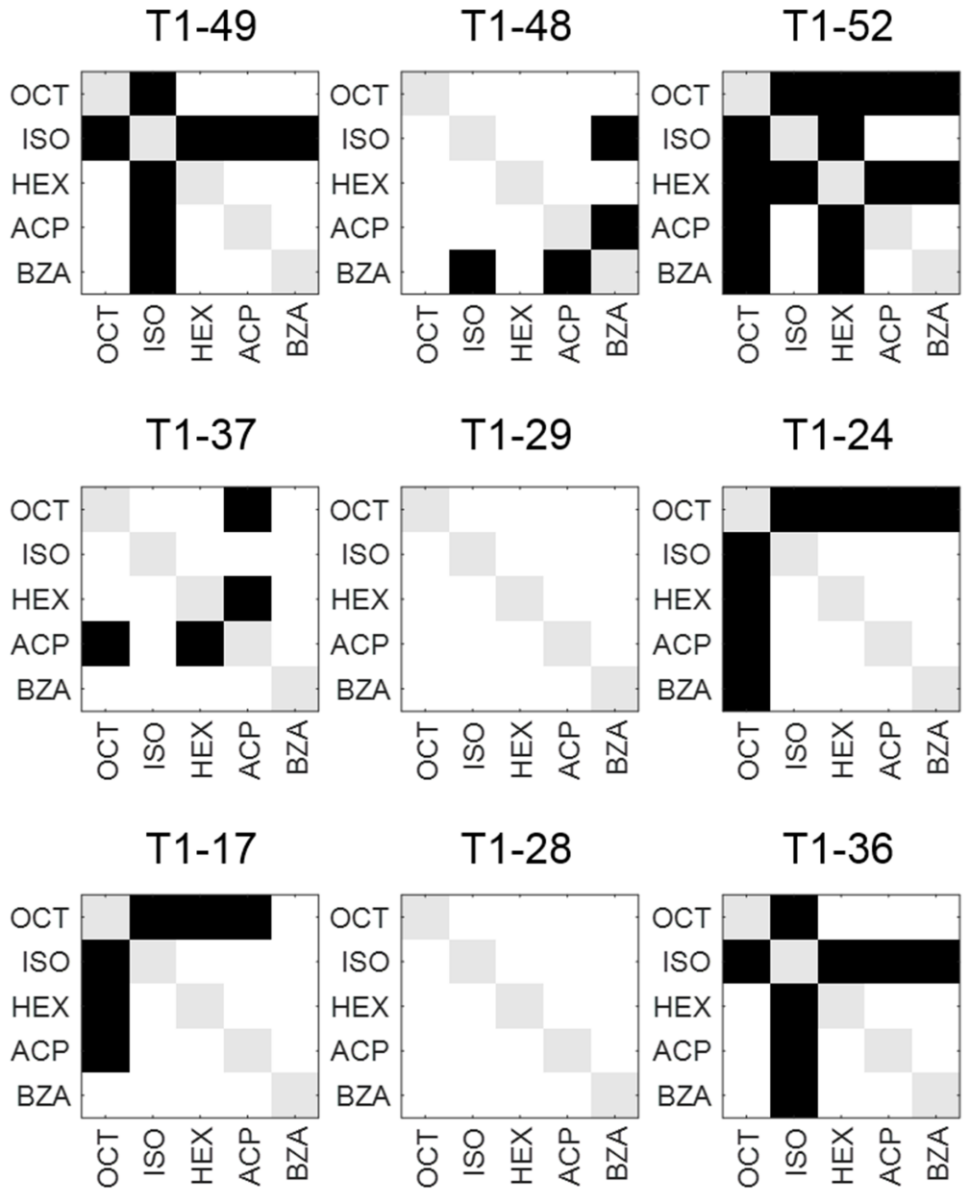
T1-49
T1-48
T1-52
T1-37
T1-29
T1-24
T1-17
T1-28
T1-36
OCT
ISO
HEX
ACP
BZA

Figure 6:

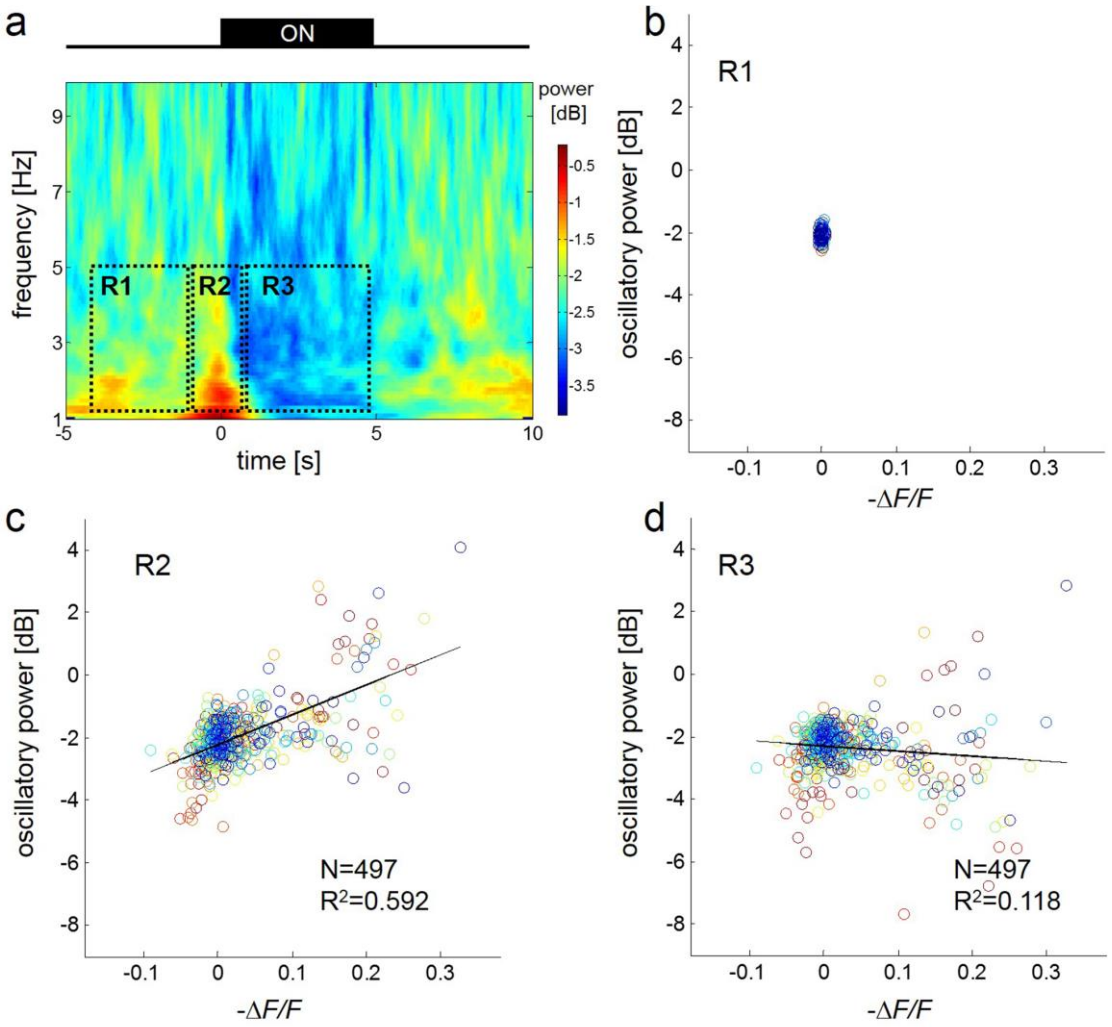
a
ON
power [dB]
frequency [Hz]
time [s]
R1
R2
R3
b
R1
oscillatory power [dB]
-ΔF/F
c
R2
oscillatory power [dB]
N=497
R²=0.592
-ΔF/F
d
R3
oscillatory power [dB]
N=497
R²=0.118
-ΔF/F

Figure 7:

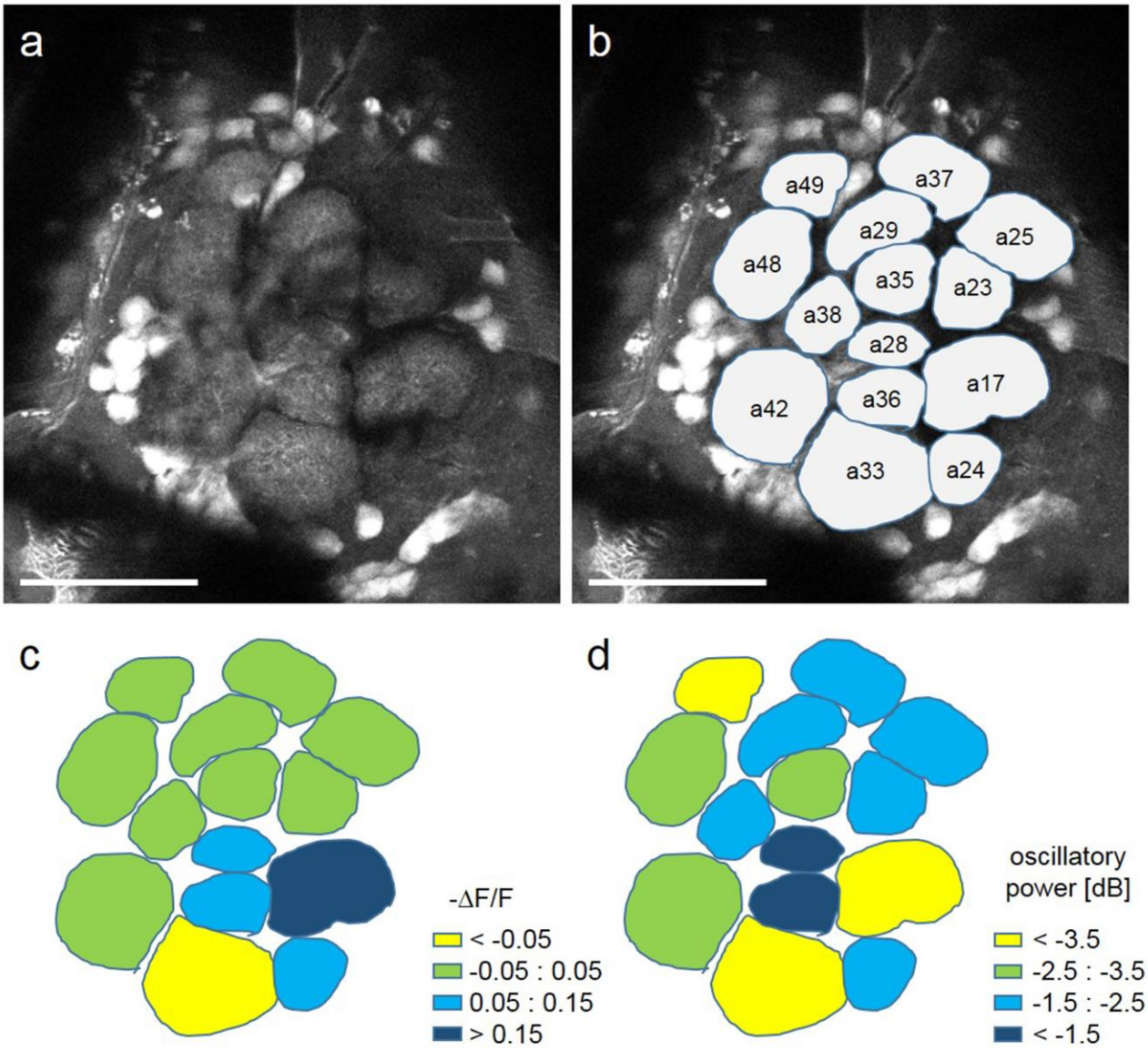
a
b
a49
a37
a29
a25
a48
a35
a23
a38
a28
a17
a42
a36
a33
a24
c
-ΔF/F
< -0.05
-0.05 : 0.05
0.05 : 0.15
> 0.15
d
oscillatory
power [dB]
< -3.5
-2.5 : -3.5
-1.5 : -2.5
< -1.5